Letter

Vertically aligned zinc oxide nanowires electrodeposited within porous polycarbonate templates for vibrational energy harvesting

Francesca L Boughey, Timothy Davies[1], Anuja Datta, Richard A Whiter, Suman-Lata Sahonta and Sohini Kar-Narayan

Department of Materials Science and Metallurgy, University of Cambridge, 27 Charles Babbage Road, Cambridge CB3 0FS, UK

E-mail: sk568@cam.ac.uk

Abstract

A piezoelectric nanogenerator has been fabricated using a simple, fast and scalable template-assisted electrodeposition process, by which vertically aligned zinc oxide (ZnO) nanowires were directly grown within a nanoporous polycarbonate (PC) template. The nanowires, having average diameter 184 nm and length 12 μm, are polycrystalline and have a preferred orientation of the [100] axis parallel to the long axis. The output power density of a nanogenerator fabricated from the as-grown ZnO nanowires still embedded within the PC template was found to be $151 \pm 25 \, \text{mW m}^{-3}$ at an impedance-matched load, when subjected to a low-level periodic (5 Hz) impacting force akin to gentle finger tapping. An energy conversion efficiency of ~4.2% was evaluated for the electrodeposited ZnO nanowires, and the ZnO–PC composite nanogenerator was found to maintain good energy harvesting performance through 24 h of continuous fatigue testing. This is particularly significant given that ZnO-based nanostructures typically suffer from mechanical and/or environmental degradation that otherwise limits their applicability in vibrational energy harvesting. Our template-assisted synthesis of ZnO nanowires embedded within a protective polymer matrix through a single growth process is thus attractive for the fabrication of low-cost, robust and stable nanogenerators.

S Online supplementary data available from stacks.iop.org/NANO/27/28LT02/mmedia

Keywords: nanogenerator, piezoelectric, zinc oxide, electrodeposition, nanowires, energy harvesting

(Some figures may appear in colour only in the online journal)

---

[1] *Present address*: University of Oxford, Department of Materials, Parks Road Oxford, OX1 3PH, UK.

1. Introduction

Since 2006, when the concept of a zinc oxide (ZnO) piezoelectric nanogenerator (NG) first appeared in the literature [1], there has been a wide range of ZnO-based devices published with different geometries and architectures. These include
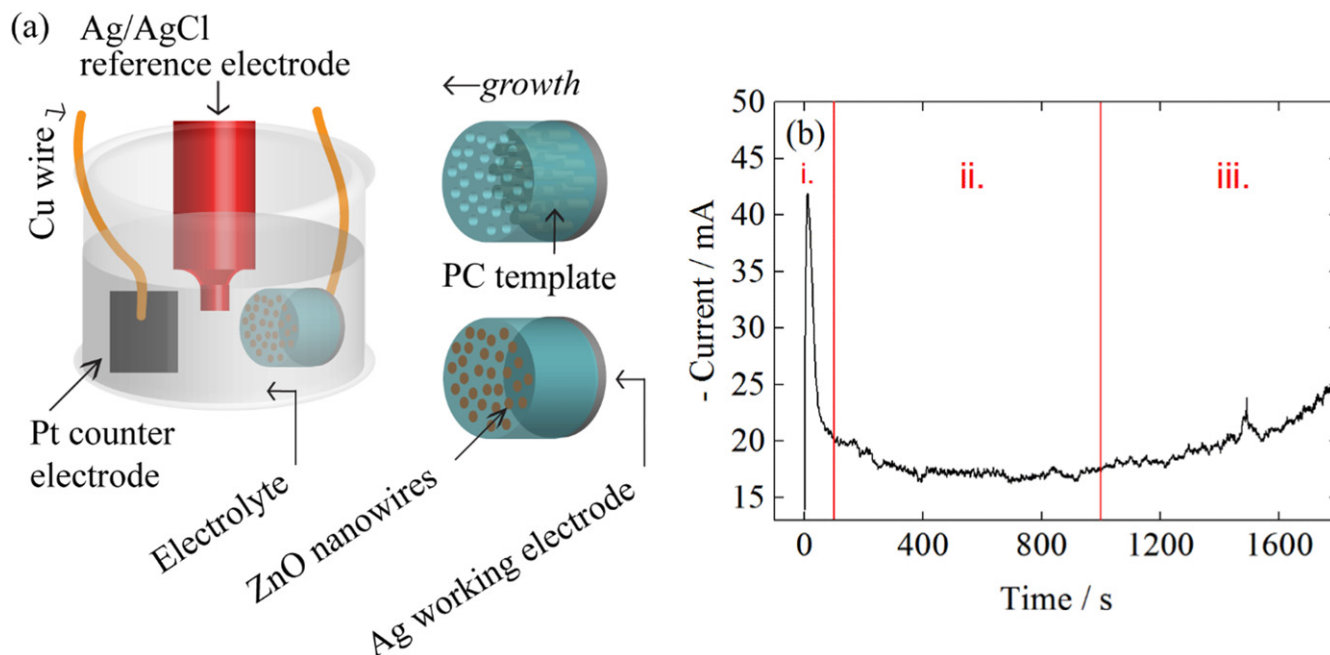
Figure 1. (a) A schematic of a nanoporous polycarbonate template showing the nanowire growth from the back silver electrode to the top of the template via electrodeposition, and a schematic of the electrodeposition set-up including the electrolyte bath and positions of the working, counter and reference electrodes. (b) Electrodeposition current plot versus time indicating the three growth regimes.

single nanowires (NWs) [2], vertical NW arrays [3, 4], lateral NW arrays [5], template-based nanotube (NT)/NW arrays [6, 7] and other morphologies [8, 9]. Alongside their use in NGs, ZnO NWs have also been studied for applications in solar cells [10, 11] and gas sensing [12]. In the context of vibrational energy harvesting, NWs outperform bulk or thin film structures due to their high aspect ratio and high surface-to-volume ratio, which provide improved sensitivity to low-amplitude ambient vibrations and reduced fragility [13]. Piezoelectric performance is typically quantified in the literature by the d_{33} value, a normal component of the piezo-electric charge coefficient, defined as the rate of change of the dielectric displacement with respect to stress at constant electric field when the applied stress is parallel to the polar-ization [14]. The NW geometry is particularly attractive in this respect as theoretical [15–19] and experimental [20] studies have suggested that the bulk value of d_{33} will vary from the equivalent NW values due to their surface-like nature, in particular that d_{33} increases as the NW diameter decreases, and similarly for the Young's modulus, Y [20]. Piezo force microscopy measurements performed on ZnO NWs reported d_{33} as 0.4–9.520. More recent studies have indicated a d_{33} increase of ∼18% in ZnO NWs as compared to bulk [21]. For bulk ZnO, experimental measurements have shown the electromechanical coupling factor, k_{33}^2 which describes how effective a piezoelectric material is at con-verting mechanical energy to electrical energy [22], to be 0.17–0.23 [23, 24] and for comparison, bulk barium titanate (BaTiO$_3$) to be 0.25 [24]. The piezoelectric performance of ZnO is therefore comparable to lead-free ceramics such as BaTiO$_3$, with ZnO having the advantage of being relatively easy to synthesize into nanostructures [25].

The size, morphology and crystallinity of ZnO NWs are determined by the exact growth mechanism [26]. Wet che-mical methods are typically relatively low-temperature, low-cost, scalable, and the least hazardous, as well as being effective at controlling size morphology and properties of the NWs. Within the wet chemical methods, electrodeposition is possibly the simplest, requiring the lowest temperature and pressure, and thus more cost-effective and scalable [26]. It is also possible to use a wide range of materials and control the growth through deposition parameters [27]. NWs grown by electrodeposition are in general found to exhibit better crys-tallinity and piezoelectric properties than those grown by other methods such as hydrothermal synthesis [28]. There are examples of polycrystalline ZnO NW arrays in the literature where the NWs consist of crystallites grown via template-assisted electrodeposition (TAED) in both anodized alumi-num oxide (AAO) [29–32] and, more recently, polycarbonate (PC) templates [33] with various orientations. In comparison, there are limited examples of single crystal [002] axis orientated TAED NW arrays although it has been shown in AAO [34] and in PC [35], and also with a growth direction perpendicular to the (101) [36] plane or no preferred orien-tation [37].

Here we present vertically aligned, high aspect-ratio polycrystalline ZnO NWs, grown via TAED with preferred orientation of the [100] axis parallel to the long axis of the NWs hence with crystal plane growth parallel to the [002] *c*-axis. With the NW array directly grown and embedded in a PC template, the resulting NG comprised a flexible ZnO–PC composite with an Ag sputtered electrode on one side and Al foil on the other. The NW electrodeposition was performed with a standard three-electrode cell directly within the PC
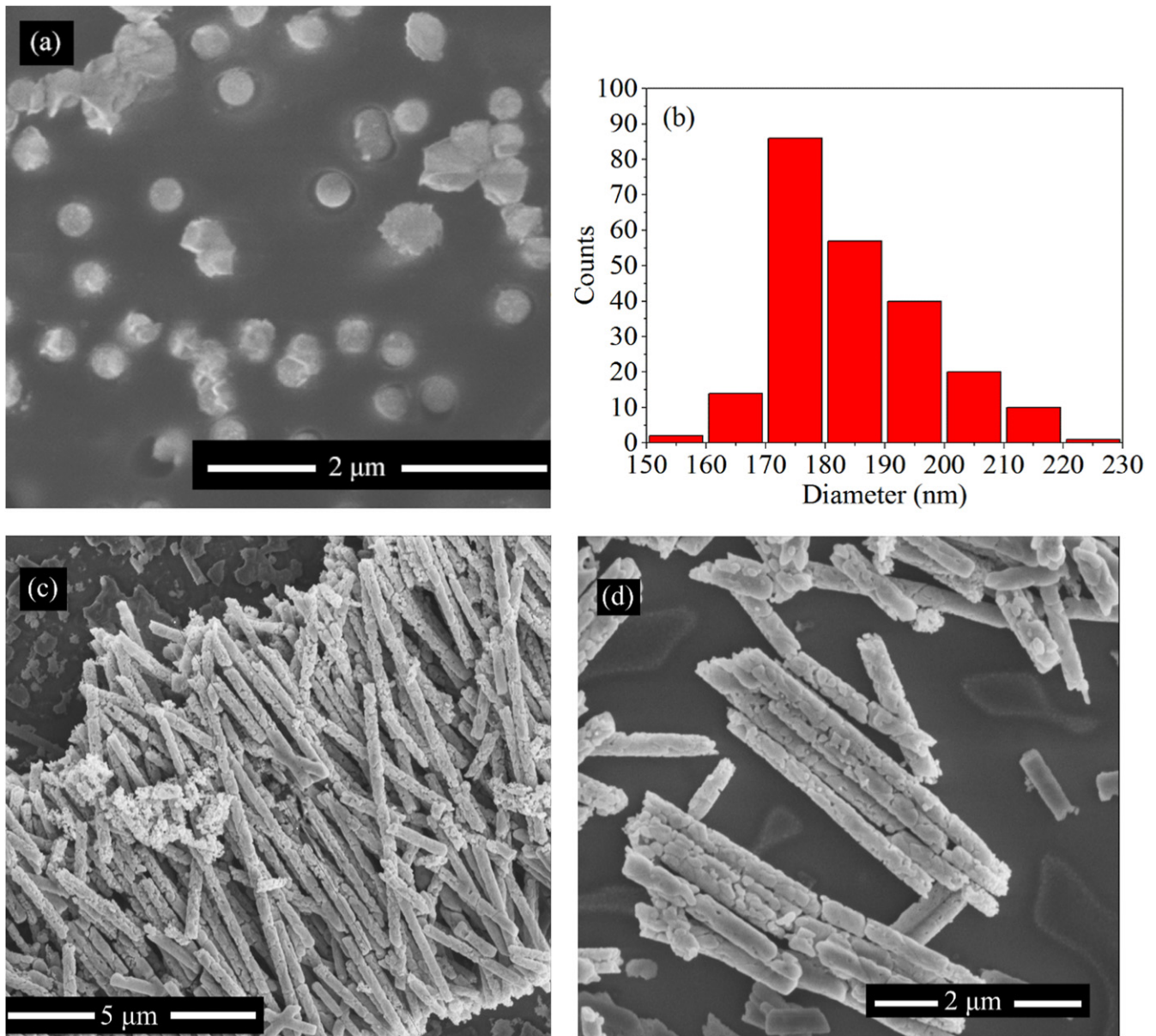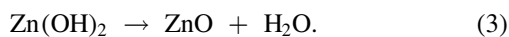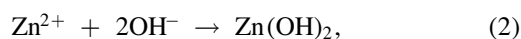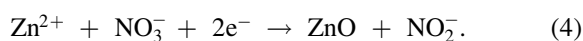
Figure 2. Scanning electron micrographs of (a) a top-down view of a small section of a zinc oxide nanowire filled polycarbonate template, (b) a histogram of the average nanowire diameter measured using images such as (a), (c) zinc oxide nanowire array after removal of the polycarbonate template and (d) a higher magnification image of several broken nanowires.

template, as shown in figure 1(a), at a fixed temperature of 75 °C and pH 4–5 with constant stirring. The potential was fixed at −1.0 V during the deposition and the transient current was recorded. The proposed growth technique [38] follows the reactions (1)–(3):

$$NO_3^- + H_2O + 2e^- \rightarrow NO_2^- + 2OH^-, \quad (1)$$

$$Zn^{2+} + 2OH^- \rightarrow Zn(OH)_2, \quad (2)$$

$$Zn(OH)_2 \rightarrow ZnO + H_2O. \quad (3)$$

The balanced reaction is therefore:

$$Zn^{2+} + NO_3^- + 2e^- \rightarrow ZnO + NO_2^-. \quad (4)$$

Thus, under an applied potential, the nitrate ions reduce to nitrite ions in an aqueous solution which produces excess

OH⁻ ions in the region close to the working electrode. This increases the local pH and both the OH⁻ ions and the Zn^{2+} ions diffuse through the pores towards the base of the template. Depending on the reaction rate of the nitrate reduction, which is determined by the applied potential, there is either instantaneous nucleation directly onto the working electrode followed by growth for relatively high potentials or there is solution supersaturation at lower potentials where the $Zn(OH)_2$, or ZnO if the temperature is above ~50 °C, precipitates in the electrolyte and then deposits onto the working electrode surface, again followed by growth [27, 38, 39]. This mechanism, which has previously been hypothesized, was recently experimentally confirmed for the first time by *in situ* transmission x-ray microscopy of electrodeposited ZnO by Tay *et al* [27].
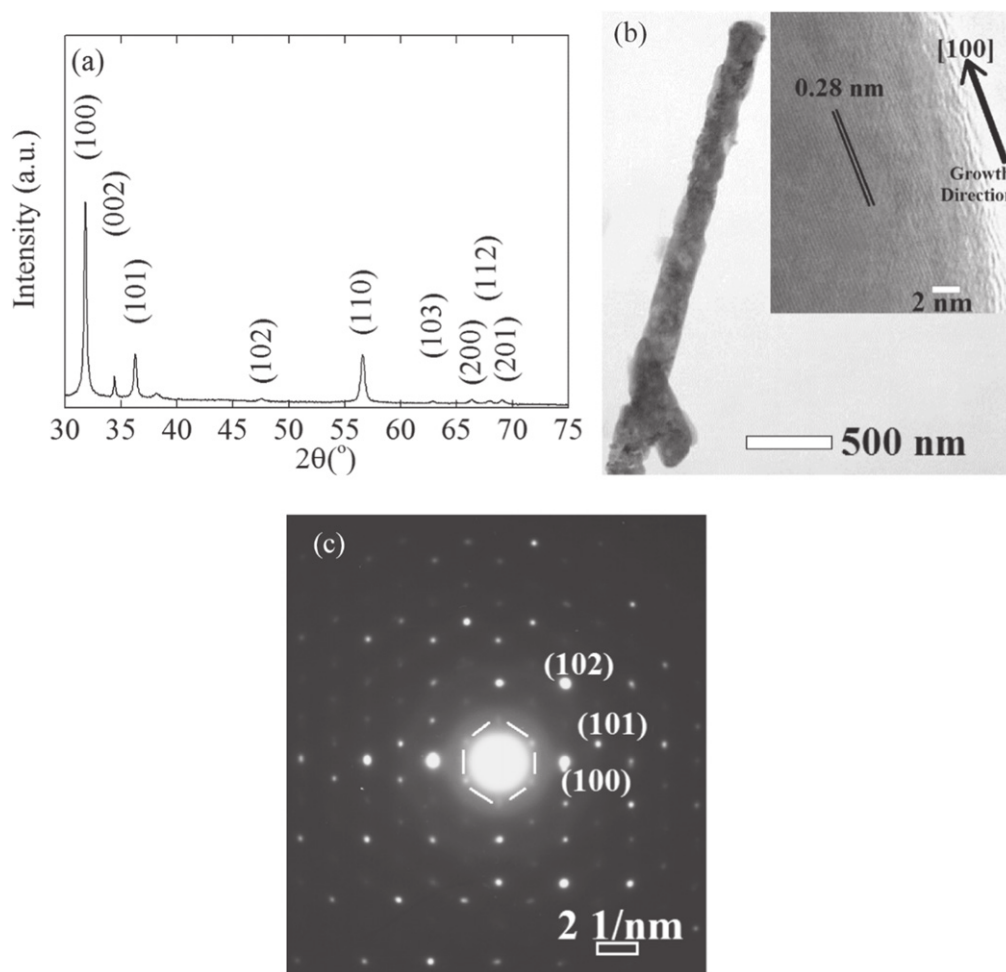
Figure 3. (a) X-ray diffraction pattern of zinc oxide nanowires in a polycarbonate template grown by electrodeposition, (b) transmission electron micrograph (TEM) of a single zinc oxide nanowire with an inset of a high resolution TEM and (c) is the selected area electron diffraction pattern of this nanowire.

The growth and the crystallinity of the NWs has been found to be affected by the choice of template, applied potential or current density, electrolyte bath composition, pH, temperature, stirring and sonication [40]. In the present study, PC rather than AAO templates were used because of the higher flexibility of the former which allows the final NG device to be more compliant and less prone to mechanical fracture. Additionally, the presence of the template reduces both the likelihood of electrical shorting when the electrodes are applied in the final NG device, as well as the likelihood of gases being adsorbed onto the surface of the NWs. This can help reduce the effect of a reduced polarization potential due to external screening of the polarization charges resulting in a reduced output voltage, without the need for surface passivation as previously reported [41, 42].

2. Methods

2.1. Fabrication of ZnO NWs

A commercially available nanoporous PC track etched membrane (Whatman® Cyclopore®) of diameter 25 mm with nominal pore diameter ~200 nm, pore length ~12 μm and porosity (4–20)% was first prepared by submerging it in deionized water and cleaned in an ultrasonic bath (U50, Ultrawave) for 3 min and subsequently dried at ~100 °C for 10 min. A ~100 nm Ag electrode was sputtered on one side using a sputter coater (K575, EMITECH) at 40 mA for 4 min. A circular shadow mask was used to sputter a ~3 cm^2 area on the ~5 cm^2 template and a Cu wire was attached to the electrode using electrically conductive adhesive transfer tape (3M™), aluminum foil (Sphere Consumer Products plc) and silver conductive paint. The electrode was then covered in polyimide tape (3M™) to prevent deposition of the back surface. Zinc nitrate hexahydrate $Zn(NO_3)_2 \cdot 6H_2O$ crystallized ⩾99.0% (Sigma-Aldrich) was dissolved in deionized water to make a 0.1 M solution, pH ≈ 4–5 (pH 510 series, Oakton instruments). The three electrodes, as described in the main text plus a magnetic follower (Fisher Scientific), were submerged in 100 ml of this solution and heated in a water bath to 75 °C. A potentiostat (VersaSTAT 4, Princeton Applied Research) was used in chronoamperometry mode: – 1 V was applied between the working electrode and the double junction Ag/AgCl (with saturated KCl solution) reference electrode (Sigma-Aldrich) for ~15 min and the
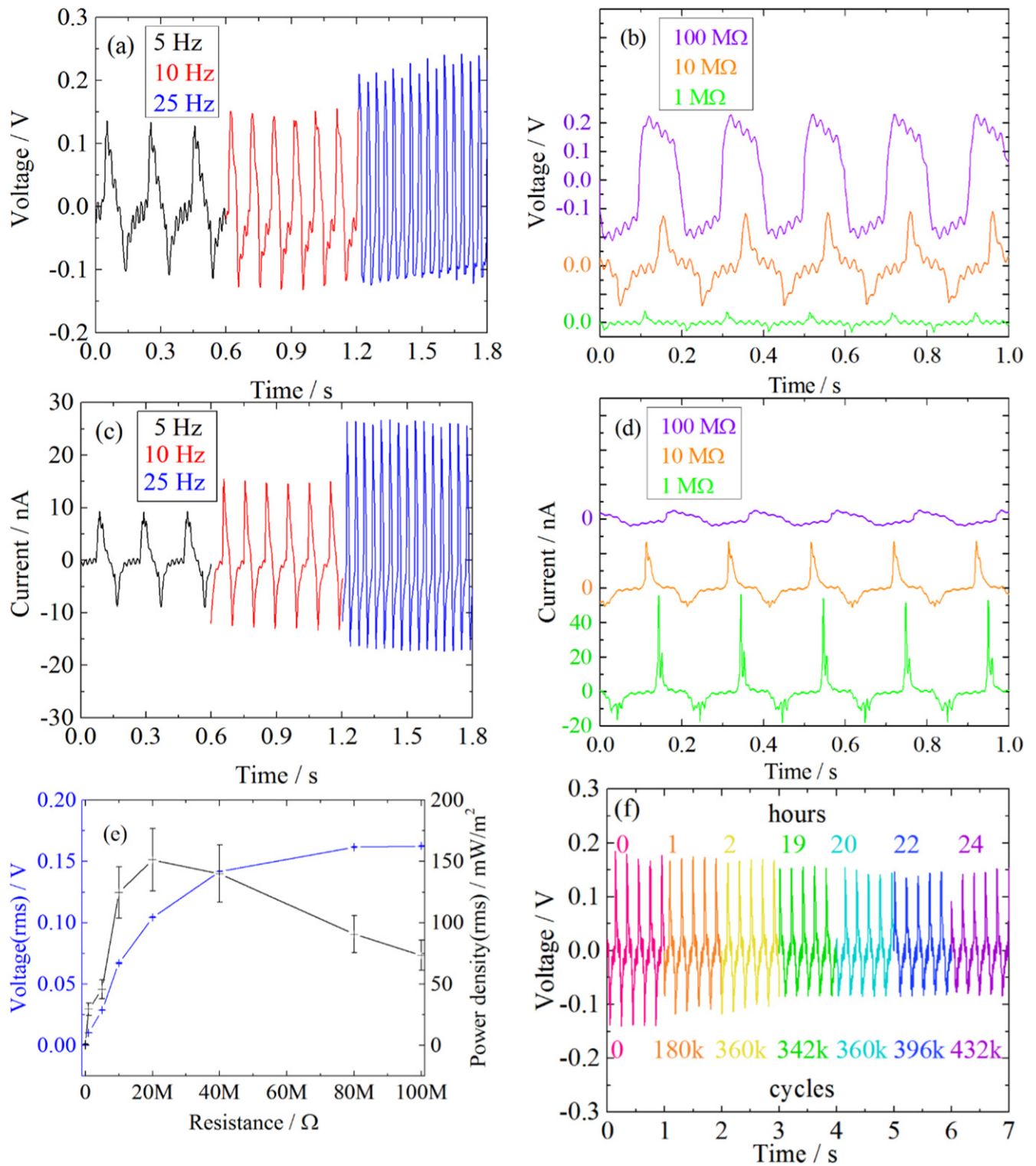
Figure 4. Electrical output of the ZnO–PC nanogenerator. (a) Voltage output at different frequencies of impact vibrations measured across a 20 MΩ resistor and (b) the voltage across different loads at 5 Hz. (c) Current output at different frequencies measured through a 20 MΩ resistor and (d) the current through different resistors at 5 Hz. (e) Root-mean-square voltage measured over ten different resistors and the corresponding power density of a single device and (f) the voltage output measured across a 10 MΩ resistor at 5 Hz after 1, 2, 19, 22 and 24 h. The amplitude of the impacting vibrations is frequency-dependent and for 5 Hz, 10 Hz and 25 Hz are 0.68 mm 0.65 mm 0.78 mm respectively.

Table 1. Electrical performance of the zinc oxide–polycarbonate nanogenerator presented here. I_{sc}, V_{oc}, P_A, P_d, P', E, χ, η_T, η_s and χ' are the average peak short-circuit current, open-circuit voltage, root-mean-square (rms) power density with respect to area, rms power density with respect to volume, specific rms power, average energy density per cycle, energy conversion efficiency, stress and strain figures of merit [22] and overall device efficiency.

I_{sc} (nA)	V_{oc} (mV)	P_A (μW m^{-2})	P_d (mW m^{-3})	P' (μW kg^{-1})	E (nJ m^{-2})	χ (%)	η_T (pJ m^{-3} Pa^{-2})	η_s (GJ m^{-3})	χ' ($\times 10^{-3}$%)
24.7 ± 0.2	283 ± 1	1.82 ± 0.03	151 ± 25	6.79 ± 0.07	372 ± 2	$\sim$4.2	$\sim$1.26	$\sim$1.40	$\sim$3.76

current flow between the working and counter electrodes (platinum foil 20 mm $\times$ 20 mm) was measured with the supplied software package (VersaStudio).

2.2. ZnO NW array characterization

Field-emission scanning electron microscopy (FE-SEM, FEI Nova NanoSEM) was used for imaging of the NWs. The NW diameters were measured by using the scaled scanning electron microscope (SEM) image (ImageJ). For the freed NWs, a small piece of the ZnO filled PC templates was placed on a SiO$_2$ wafer and then the PC template was dissolved with a few drops of ReagentPlus® 99% chlorobenzene (Sigma-Aldrich). The sample was placed on a hotplate (C-MAG HS 4, IKA®) for $\sim$5 min to speed up the evaporation of the solvent and then placed in a furnace (Carbolite Furnaces) for 30 min at 500 °C at a heating rate of 1 °C min^{-1} to burn away the entire PC template. All samples were coated in palladium using a sputter coater at 40 mA for 20 s. X-ray diffraction (XRD) analysis was performed with a diffractometer (D8 Advance, Bruker) with a Cu Kα source and a non-rotating sample holder. For the high resolution TEM (HRTEM) (JEOL 4000EXII) imaging, the sample preparation was the same as for SEM except that the white-brown powder left after burning the template was dispersed in 0.5 ml of absolute ethanol (analytical reagent grade, Fisher Scientific). A droplet was then drop cast onto a Cu coated TEM grid and naturally dried in air for 20 min.

2.3. Fabrication and testing of the NG

From a ZnO NW filled PC template, a second electrode was added using firstly a layer of electrically conductive adhesive transfer tape with a piece of Al foil on top of the same area as the original electrode. A second Cu wire was attached with silver paint to this electrode. The energy harvesting set-up used to measure the voltage and current characteristics of the NG has been previously described [43] with a digital multimeter (Keithley 2002) for voltage measurements and a picoammeter (Keithley 6487) for current measurements. The whole setup was also enclosed in a grounded Al box which acts as a Faraday cage.

3. Results and discussion

Figure 1(b) demonstrates the typical current versus time plot for electrodepositions at −1.0 V. Immediately after the

potential is applied (phase i), instantaneous nucleation occurs on the working electrode and this surface charge forms the first layer of the electric double layer, causing the current to suddenly increase. The sudden drop in current is then due to the formation of the second diffusion layer as the Zn ions flow towards the electrode and simultaneously reduce to form ZnO and precipitate on the surface. This causes a concentration gradient of Zn ions, decreasing towards the working electrode, thereby causing more of them to flow towards the electrode and continue to deposit. As the pores are filled in this way the current is approximately constant because the surface area exposed to the electrolyte is constant (phase ii). Once the pores are filled, the NWs emerge from the template and begin to form a film on the top and this steady increase in surface area causes a steady current increase (phase iii) [39]. The deposition was stopped at the onset of this stage in order to have an array of NWs without being connected by a film.

Figure 2(a) shows a top-down SEM image of the NW-filled PC template showing a clear difference in contrast between the template and the ZnO. The presence of Zn is further confirmed by energy dispersive x-ray analysis in supplementary data S1. The black holes observed indicate regions where the NWs have not reached the surface or not filled the pores. This could be due to organic contaminants or trapped air in the pores. Slightly overgrown NWs are also visible in this image. The diameter distribution is displayed in figure 2(b), which gives an average NW diameter of (184 $\pm$ 1) nm. The average pore size is $\sim$(227 $\pm$ 92) nm [7] indicating that the NWs grow to less than the diameter of the pores themselves. The nominal thickness of the template is $\sim$12 μm and after freeing the NWs from the template through a controlled burning process, the approximate length is $\sim$10 μm as can be seen in figure 2(c). This difference is likely due to breakages of the NWs from the electrode during sample preparation. Figure 2(d) shows how the NWs break up into smaller pieces when released, and hence the template serves to protect the NWs while they are still embedded.

Figure 3(a) shows an XRD plot of the ZnO NWs deposited at −1.0 V. The presence of other peaks besides the preferred orientation indicates that the ZnO NWs are either polycrystalline with an overall preferred orientation or they could be single crystals all with different orientations but most having the same preferred orientation. The texture coefficient (TC) of the (100) peak is 3.9 in this range and so a clear preferred orientation is visible (see supplementary data S2). A deposition at −1.2 V was also performed where [002] preferred orientation was found before cleaning the top

surface of the template with HCl, which switches to [100] axis orientation after cleaning. (The XRD results before and after cleaning at -1.2 V are presented in supplementary data figure S2.) At this higher voltage, the growth is faster which leads to the formation of a film on top of the template. This does not occur at the lower potential as long as the deposition is stopped at the correct time.

Figure 3(b) shows the TEM image of a single freed ZnO NW. The NW is composed of large ZnO polygonal crystallites of sizes between 100 and 150 nm (one dimension). The inset shows the HRTEM image of one ZnO crystallite, which indicates the lattice fringe spacing of plane (100) = 0.28 nm of phase-pure ZnO. The growth direction of the NW is along the [100] axis which is parallel to the long axis of the NW. Figure 3(c) shows the selected area electron diffraction pattern of the ZnO NWs that mostly shows a single crystalline pattern with a superimposed polycrystalline ring pattern from the adjacent polycrystalline crystallites of ZnO. Major diffraction planes such as (100), (101) and (102) could be indexed. The diffraction spots reveal a hexagonal lattice structure of ZnO NWs. From the XRD, SEM and TEM measurements it can be stated that the PC template can influence the growth rate of the different crystal planes. Without the template, NWs with the [002] axis oriented parallel to the long axis tend to grow because the high surface energy polar faces grow faster than the non-polar faces. This may be altered by the PC pore surface energy and in this case, the NWs are formed of single crystal nanoparticles with the [002] axis parallel to the plane of the template stacked on top of one another within each pore.

A NG based on the ZnO NWs grown by TAED was fabricated and the electrical output was measured in response to periodic impacting by an oscillating mechanical arm at a set frequency in a bespoke energy harvesting measurement setup that has been previously described in [43]. An integrated schematic of the NG consisting of vertically aligned ZnO NWs embedded within a PC template is presented in supplementary data S3, which shows how the NG was subjected to a periodic impacting force parallel to the long axis of the NWs. The mechanical excitation was such that the NWs were being periodically compressed along their lengths and then released, resulting in the measured electrical output. The ZnO–PC nanocomposite NG is an example of a stress-driven NG [22, 44], as the ZnO NWs have a relatively large area-weighted stiffness compared to the PC template in which they are embedded.

Figure 4(a) displays the voltage measured across an impedance-matched resistance of 20 MΩ at 5 Hz, 10 Hz and 25 Hz and in (b) across 1 MΩ, 10 MΩ and 100 MΩ resistors at 5 Hz (see supplementary data S4 for the circuit diagram). The peak-to-peak voltage (V_{pp}) increases with frequency due to higher acceleration, and hence force, of the impacting arm. As the resistive load increases the voltage drop and hence V_{pp} increases. The width of the peaks widens as the load increases due to the longer time constant (product of resistance and capacitance) resulting in slower charge and discharge. Figures 4(c)–(d) show the equivalent plots for current measured in series with the NG and the resistors. The output

power was measured across ten different resistors and is plotted alongside root-mean-square voltage (V_{rms}) across each load in figure 4(e). The peak in output power occurred under impedance-matched conditions across a resistor ∼20 MΩ. Figure 4(f) shows the fatigue characteristics of the NG under continuous impacting through 24 h. After an initial ∼11% decrease in V_{pp} within the first 2 h, the NG maintained a reasonably constant output voltage throughout the fatigue test, and the device did not show any visible physical damage.

Table 1 outlines the full electrical characteristics with an estimated input energy of ∼3 μJ per cycle of the impacting arm (see supplementary data S4 and S5). Additionally, energy conversion efficiency and figures of merit, as defined in [22], were evaluated for the ZnO NWs grown by TAED (see supplementary data S4), and found to be comparable to previously reported values, while an overall device efficiency was also calculated as shown in supplementary data S5 and reported in table 1. The effect of crystallinity of the NWs on NG performance has previously been studied, and indicates that as the size of the crystallites within ZnO NWs [45] or nanotubes [6] increases, the voltage and current output increases. This is due to the decrease in the number of grain boundaries and defects for larger crystallites, which is seen in XRD patterns as the narrowing of the preferred orientation peak [6].

4. Conclusion

In summary, TAED was used to grow a vertically aligned ZnO NW array with [100] axis preferred orientation embedded in a PC template, which was then directly fabricated into a piezoelectric NG for applications in vibrational energy harvesting. This method is simple, cost-effective and scalable, with minimal steps required for the fabrication of a robust NG with good energy harvesting performance, as evidenced by voltage and current data at varying impacting frequencies and measured across varying loads, for up to 24 continuous hours. The aligned nature of the embedded nanowires ensures good piezoelectric performance across the entire device under impacting, while the PC template ensures mechanical stability and longevity of the device. The confined growth process achieved through TAED thus overcomes problems typically arising due to mechanical and/or environmental degradation in ZnO-based nanostructures that limits their applicability in vibrational energy harvesting. Importantly, the TAED method for growing ZnO nanowires and subsequent NG fabrication require only a single growth process and minimal post-deposition processing, and can thus be easily scaled up for low-cost and long-lasting energy harvesting applications.

References

[1] Wang Z L and Song J 2006 Piezoelectric nanogenerators based on zinc oxide nanowire arrays *Science* **312** 242–6

[2] Yang R, Qin Y, Dai L and Wang Z L 2009 Power generation with laterally packaged piezoelectric fine wires *Nat. Nanotechnol.* **4** 34–9

[3] Wang X, Song J, Liu J and Wang Z L 2007 Direct-current nanogenerator driven by ultrasonic waves *Science* **316** 102–5

[4] Hu Y, Zhang Y, Xu C, Lin L, Snyder R L and Wang Z L 2011 Self-powered system with wireless data transmission *Nano Lett.* **11** 2572–7

[5] Zhu G, Yang R, Wang S and Wang Z L 2010 Flexible high-output nanogenerator based on lateral ZnO nanowire array *Nano Lett.* **10** 3151–5

[6] Stassi S, Cauda V, Ottone C, Chiodoni A, Pirri C F and Canavese G 2015 Flexible piezoelectric energy nanogenerator based on ZnO nanotubes hosted in a polycarbonate membrane *Nano Energy* **13** 474–81

[7] Ou C, Sanchez-Jimenez P, Datta A, Boughey F L, Whiter R A, Sahonta S and Kar-Narayan S 2016 Template-assisted hydrothermal growth of aligned zinc oxide nanowires for piezoelectric energy harvesting applications *ACS Appl. Mater. Interfaces* (submitted) (doi:10.1021/acsami.6b04041)

[8] Qin Y, Wang X and Wang Z L 2008 Microfibre-nanowire hybrid structure for energy scavenging *Nature* **451** 809–13

[9] Cauda V, Stassi S, Lamberti A, Morello M, Fabrizio Pirri C and Canavese G 2015 Leveraging ZnO morphologies in piezoelectric composites for mechanical energy harvesting *Nano Energy* **18** 212–21

[10] Baxter J B, Walker A M, Ommering K van and Aydil E S 2006 Synthesis and characterization of ZnO nanowires and their integration into dye-sensitized solar cells *Nanotechnology* **17** S304–12

[11] Dymshits A, Iagher L and Etgar L 2016 Parameters influencing the growth of ZnO nanowires as efficient low temperature flexible perovskite-based solar cells *Materials* **9** 60

[12] Lin C, Chang S-J, Chen W-S and Hsueh T-J 2016 Transparent ZnO-nanowire-based device for UV light detection and ethanol gas sensing on c-Si solar cell *RSC Adv.* **6** 11146–50

[13] Chen X, Xu S, Yao N and Shi Y 2010 1.6 V nanogenerator for mechanical energy harvesting using PZT nanofibers *Nano Lett.* **10** 2133–7

[14] Crossley S, Whiter R A and Kar-Narayan S 2014 Polymer-based nanopiezoelectric generators for energy harvesting applications *Mater. Sci. Technol.* **30** 1613–24

[15] Xiang H J, Yang J, Hou J G and Zhu Q 2006 Piezoelectricity in ZnO nanowires: a first-principles study *Appl. Phys. Lett.* **89** 223111

[16] Xin J, Zheng Y and Shi E 2007 Piezoelectricity of zinc-blende and wurtzite structure binary compounds *Appl. Phys. Lett.* **91** 112902

[17] Mitrushchenkov A, Linguerri R and Chambaud G 2009 Piezoelectric properties of AlN, ZnO, and Hg$_x$Zn$_{1-x}$O nanowires by first-principles calculations *J. Phys. Chem. C* **113** 6883–6

[18] Agrawal R and Espinosa H D 2011 Giant piezoelectric size effects in zinc oxide and gallium nitride nanowires, a first principles investigation *Nano Lett.* **11** 786–90

[19] Yan Z and Jiang L 2011 Surface effects on the electromechanical coupling and bending behaviours of piezoelectric nanowires *J. Phys. D: Appl. Phys.* **44** 075404

[20] Espinosa H D, Bernal R A and Minary-Jolandan M 2012 A review of mechanical and electromechanical properties of piezoelectric nanowires *Adv. Mater.* **24** 4656–75

[21] Tamvakos D, Lepadatu S, Antohe V-A, Tamvakos A, Weaver P M, Piraux L, Cain M G and Pullini D 2015 Piezoelectric properties of template-free electrochemically grown ZnO nanorod arrays *Appl. Surf. Sci.* **356** 1214–20

[22] Crossley S and Kar-Narayan S 2015 Energy harvesting performance of piezoelectric ceramic and polymer nanowires *Nanotechnology* **26** 344001

[23] Crisler D F, Cupal J J and Moore A R 1968 Dielectric, piezoelectric, and electromechanical coupling constants of zinc oxide crystals *Proc. IEEE* **56** 225–6

[24] Jaffe H and Berlincourt D A 1965 Piezoelectric transducer materials *Proc. IEEE* **53** 1372–86

[25] Schmidt-Mende L and MacManus-Driscoll J L 2007 ZnO-nanostructures, defects, and devices *Mater. Today* **10** 40–8

[26] Xu S and Wang Z L 2011 One-dimensional ZnO nanostructures: solution growth and functional properties *Nano Res.* **4** 1013–98

[27] Tay S E R, Goode A E, Weker J N, Cruickshank A A, Heutz S, Porter A E, Ryan M P and Toney M F 2016 Direct in situ observation of ZnO nucleation and growth via transmission x-ray microscopy *Nanoscale* **8** 1849–53

[28] Leprince-Wang Y 2015 *Piezoelectric ZnO Nanostructure for Energy Harvesting* (New York: Wiley)

[29] Zheng M J, Zhang L D, Li G H and Shen W Z 2002 Fabrication and optical properties of large-scale uniform zinc oxide nanowire arrays by one-step electrochemical deposition technique *Chem. Phys. Lett.* **363** 123–8

[30] Öztürk S, Kılınç N, Taşaltın N and Öztürk Z Z 2012 Fabrication of ZnO nanowires and nanorods *Physica* E **44** 1062–5

[31] Chen Y-H, Shen Y-M, Wang S-C and Huang J-L 2014 Fabrication of one-dimensional ZnO nanotube and nanowire arrays with an anodic alumina oxide template via electrochemical deposition *Thin Solid Films* B **570** 303–9

[32] Ottone C, Bejtka K, Chiodoni A, Farías V, Roppolo I, Canavese G, Stassi S and Cauda V 2014 Comprehensive study of the templating effect on the ZnO nanostructure formation within porous hard membranes *New J. Chem.* **38** 2058–65

[33] Movsesyan L, Schubert I, Yeranyan L, Trautmann C and Toimil-Molares M E 2016 Influence of electrodeposition parameters on the structure and morphology of ZnO nanowire arrays and networks synthesized in etched ion-track membranes *Semicond. Sci. Technol.* **31** 014006

[34] Gómez H C S, Cataño F A, Altamirano H and Burgos A 2014 Template assisted electrodeposition of highly oriented ZnO nanowire arrays and their integration in dye sensitized solar cells *J. Chilean Chem. Soc.* **59** 2447–50

[35] Leprince-Wang Y, Bouchaib S, Brouri T, Capo-Chichi M, Laurent K, Leopoldes J, Tusseau-Nenez S, Lei L and

Chen Y 2010 Fabrication of ZnO micro- and nano-structures by electrodeposition using nanoporous and lithography defined templates *Mater. Sci. Eng.* B **170** 107–12

[36] Lai M and Riley D J 2006 Templated electrosynthesis of zinc oxide nanorods *Chem. Mater.* **18** 2233–7

[37] Leprince-Wang Y, Yacoubi-Ouslim A and Wang G Y 2005 Structure study of electrodeposited ZnO nanowires *Microelectron. J.* **36** 625–8

[38] Mentar L, Baka O, Khelladi M R, Azizi A, Velumani S, Schmerber G and Dinia A 2014 Effect of nitrate concentration on the electrochemical growth and properties of ZnO nanostructures *J. Mater. Sci., Mater. Electron.* **26** 1217–24

[39] Sharma S K, Rammohan A and Sharma A 2010 Templated one step electrodeposition of high aspect ratio n-type ZnO nanowire arrays *J. Colloid Interface Sci.* **344** 1–9

[40] Skompska M and Zarębska K 2014 Electrodeposition of ZnO nanorod arrays on transparent conducting substrates-a review *Electrochim. Acta* **127** 467–88

[41] Jalali N, Briscoe J, Woolliams P, Stewart M, Weaver P M, Cain M and Dunn S 2013 Passivation of zinc oxide nanowires for improved piezoelectric energy harvesting devices *J. Phys.: Conf. Ser.* **476** 012131

[42] Jalali N, Woolliams P, Stewart M, Weaver P M, Cain M G, Dunn S and Briscoe J 2014 Improved performance of p–n junction-based ZnO nanogenerators through CuSCN-passivation of ZnO nanorods *J. Mater. Chem.* A **2** 10945–51

[43] Whiter R A, Narayan V and Kar-Narayan S 2014 A scalable nanogenerator based on self-poled piezoelectric polymer nanowires with high energy conversion efficiency *Adv. Energy Mater.* **4** 1400519

[44] Wu W 2016 High-performance piezoelectric nanogenerators for self-powered nanosystems: quantitative standards and figures of merit *Nanotechnology* **27** 112503

[45] Chang C-J, Lee Y-H, Dai C-A, Hsiao C-C, Chen S-H, Nurmalasari N P D, Chen J-C, Cheng Y-Y, Shih W-P and Chang P-Z 2011 A large area bimaterial sheet of piezoelectric nanogenerators for energy harvesting: effect of RF sputtering on ZnO nanorod *Microelectron. Eng.* **88** 2236–41